Assessment of Liver Tissue After Radiofrequency Ablation: Findings with Different Imaging Procedures

Gerald Antoch, MD[1]; Florian M. Vogt, MD[1]; Patrick Veit, MD[1]; Lutz S. Freudenberg, MD[2]; Nina Blechschmid, DVM[1]; Olaf Dirsch, MD[3]; Andreas Bockisch, MD, PhD[2]; Michael Forsting, MD[1]; Jörg F. Debatin, MD, MBA[1]; and Hilmar Kuehl, MD[1]

[1]Department of Diagnostic and Interventional Radiology, University Hospital Essen, Essen, Germany; [2]Department of Nuclear Medicine, University Hospital Essen, Essen, Germany; and [3]Department of Pathology, University Hospital Essen, Essen, Germany

Our goal was to assess the typical appearance of normal liver tissue immediately after radiofrequency ablation (RF-ablation) when imaged with contrast-enhanced ultrasound, CT, MRI, ^{18}F-FDG PET, and PET/CT. **Methods:** Nineteen RF-ablation sessions were performed on nontumorous liver tissue of 10 Göttingen Mini Pigs. CT, ultrasound, MRI, ^{18}F-FDG PET, and PET/CT were performed immediately after the intervention. All imaging procedures were evaluated qualitatively for areas of increased contrast enhancement (morphologic imaging) and regions of elevated tracer uptake (functional imaging). Images were assessed quantitatively by determination of ratios ($r_{p/p}$) comparing contrast enhancement/tracer uptake in the periphery of the necrosis with contrast enhancement/tracer uptake of normal liver parenchyma. **Results:** On morphologic imaging, an increase in contrast enhancement surrounding the ablative necrosis was detected in all lesions. Quantification of this area of increased contrast enhancement revealed ratios of $r_{p/p} = 1.57 \pm 0.2$ for CT and $r_{p/p} = 1.57 \pm 0.19$ for MRI. On PET and PET/CT, homogeneous tracer utilization was found surrounding all lesions. There were no areas of a focal or rim-like increase in glucose metabolism. The ratio $r_{p/p}$ was found to be 1.05 ± 0.08 for functional data. Histologic examination revealed pooling of blood in the sinusoids of the lesion's periphery that was caused by outflow obstruction due to the central necrosis. **Conclusion:** On morphologic imaging, a rim-like increase of contrast enhancement was found immediately after RF-ablation resembling peripheral hyperperfusion. This area of contrast enhancement may hamper detection of residual tumor. On the basis of homogeneous tracer distribution surrounding the area of necrosis, PET and PET/CT may serve for early assessment of patients after RF-ablation.

Key Words: radiofrequency ablation; liver; ^{18}F-FDG PET; PET/CT

J Nucl Med 2005; 46:520–525

Received Aug. 10, 2004; revision accepted Nov. 17, 2004.

For correspondence or reprints contact: Gerald Antoch, MD, Department of Diagnostic and Interventional Radiology, University Hospital Essen, Hufelandstrasse 55, 45122 Essen, Germany.

E-mail: gerald.antoch@uni-essen.de

Minimally invasive interventional therapies of primary and secondary liver lesions are increasingly being considered attractive alternatives to surgery (*1–6*). Of these interventional procedures, radiofrequency ablation (RF-ablation) has emerged as the most widely accepted for both palliative and curative strategies (*2,7,8*). Its action is based on the application of an alternating electric current causing thermal coagulative necrosis of malignant cells. For patients with hepatocellular carcinoma, survival rates after RF-ablation have been reported to reach 93%, 62%, and 41% at 12, 24, and 36 mo, respectively (*9*). Thus, survival rates after RF-ablation are comparable to patient survival after surgical tumor resection.

Ablative treatment success is strongly dependent on ensuring complete tumor destruction. Beyond accurate placement of the ablative probe in the center of the lesion, the latter requires a thorough understanding of the ablative range (*7,10*). Considerable inter- and intratissue variability combined with the risk of suboptimal placement of the ablative device may lead to insufficient heating and thus the persistence of viable tumor cells after therapy. Waiting until local tumor growth becomes manifest carries a high risk of further metastatic spread.

To limit the risk of residual tumor, much effort has been expended on the identification of an imaging technique that permits early posttherapeutic localization of surviving tumor tissue. Virtually all attempts based on ultrasound (US), CT, or MRI have been thwarted by the immediately increased contrast enhancement in the periphery of the ablative necrosis, reflecting postinterventional hyperemia or tissue regeneration (*11–15*).

Although functional imaging with ^{18}F-FDG PET has revealed promising results regarding the detection of residual tumor after RF-ablation (*16,17*), tissue regeneration has also been shown to present as areas of increased glucose metabolism on ^{18}F-FDG PET (*18–20*). Thus, even on ^{18}F-FDG PET, the differentiation of local tissue regeneration from residual tumor may be difficult since both go along with

increased glucose metabolism (*17,20*). As tissue regeneration typically requires several days to develop, ^{18}F-FDG PET performed immediately after the ablation can be expected to reveal normal liver glucose metabolism in the zone surrounding the necrosis. The effect of the RF current on the ^{18}F-FDG PET characteristics of normal liver tissue in the periphery in the induced necrosis has, however, not yet been evaluated. At least theoretically, peripheral liver cells may react to heat by an increase in cell metabolism, causing hot spots on ^{18}F-FDG PET (*21,22*) that could not be differentiated from residual tumor.

This study was performed to assess the typical appearance of normal liver tissue immediately after RF-ablation when imaged with ^{18}F-FDG PET, ^{18}F-FDG PET/CT, contrast-enhanced US, CT, and MRI. RF-ablation was performed on nontumorous liver tissue of 10 Göttingen Mini Pigs and correlated with histopathology of the ablative necroses.

MATERIALS AND METHODS

Animal Model

The study was conducted on 10 male Göttingen Mini Pigs (30–45 kg) who underwent 2 applications of RF- ablation to the right and left liver lobes during the same session. The animals were kept in sheltered runs at the central animal facility and received a standard pig meal ad libidum. Before the intervention and the subsequent imaging procedures, the animals fasted for a minimum of 8 h. Blood glucose samples were collected before the intervention and imaging. For the intervention and imaging procedures, the animals were sedated by injecting midazolam hydrochloride (Dormicum; Hoffmann-La Roche AG) via an intravenous cannula placed in an ear's vein. Analgesia was administered intermittently using fentanyldihydrogencitrate (Fentanyl Hexal; Hexal AG). The animal study was approved by the supervising state agency (license number: G680/02) and was performed in full accordance with all state and federal guidelines.

RF-Ablation

One lesion each to the right and left part of the liver was planned in each pig. After preparing a sterile field, RF-ablation was performed with the Cool-tip system (Radionics) featuring a dual-lumen, internally cooled electrode to prevent tissue charring (*23*). Internal cooling of the electrode is achieved by continuous perfusion of the lumen with cooled saline. A single needle (17 gauge) with a 3-cm distal tip exposure was chosen for all interventions. The probe length was either 10 or 15 cm based on the individual anatomic situation. Two grounding pads were placed on the abdominal wall of each pig. The RF current was generated by a commercially available 200-W power supply (Radionics). RF-ablation was performed over a period of 20 min per lesion with the generator continuously monitoring tissue impedance and adjusting power output. When terminating each ablation, the saline perfusion was stopped to increase needle tip temperatures to 60°C. Finally, the needle was retracted slowly for cauterization of the needle track.

Imaging Procedures

All imaging procedures were performed within 90 min after completion of the RF ablation. They were performed in random order.

PET/CT. Combined PET/CT was performed on a biograph (Siemens Medical Solutions), which is composed of a dual-slice spiral CT and a full-ring PET tomograph. The PET component has an in-plane spatial resolution of 4.6 mm and an axial field of view of 15.5 cm for 1 table position. PET images are acquired in 3-dimensional mode. The CT has a minimum gantry rotation time of 800 ms and a maximal scan time of 100 s. CT and PET datasets can be viewed separately or after image fusion on a computer workstation.

CT images of the liver were acquired in a supine position with 130 mA, 130 kV, a slice width of 5 mm, and a table feed of 8 mm per gantry rotation. Images were reconstructed at 2.4-mm increments. CT was performed nonenhanced as well as contrast enhanced in the arterial phase (30-s delay) and portal venous phase (50-s delay) after administration of 70 mL of an iodinated contrast agent (flow-rate, 3 mL/s) (Xenetix 300, 300 mg iodine/mL; Guerbet GmbH) with an automated injector (Liebel).

PET images were acquired in the supine position 60 min after administering 250 MBq of ^{18}F-FDG covering the same field of view as the CT. Blood glucose levels were ensured to be within the normal range before injection of the radioactive tracer. The time to acquire a single bed position was set to 7 min. PET images were corrected for attenuation based on the nonenhanced CT data (*24*). Images were scatter corrected and iteratively reconstructed (2 iterations, 8 subsets).

US. Contrast-enhanced US was performed in a supine position on a Sequoia system (Acuson) with a curved-array 2.5- to 5-MHz transducer. Imaging was performed before and after intravenous bolus injection of 2.5 mL of a microbubble-based US contrast agent (Sonovue; Bracco International) per lesion. All images of the 2 lesions were generated nonenhanced as well as contrast enhanced in the arterial and portal venous phase. Contrast-enhanced image acquisition was performed using a low mechanical index (0.2). Images were stored digitally as well as on videotape.

MRI. MR images were acquired on a 1.5-T Sonata System (Siemens Medical Solutions). All pigs were placed on the examination table in a supine position with the field of view defined for the liver. First, noncontrast–enhanced images were acquired with respiratory gating using T1-weighted (repetition time [TR]/echo time [TE], 124/1.8) and T2-weighted sequences (TR/TE, 1,200/60) with a section width of 7 mm. Subsequently, a paramagnetic contrast agent (Multihance; Bracco) was administered intravenously at 2 mL/s with a dose of 0.2 mmol/kg. Four 3-dimensional datasets (TR/TE, 3.0/1.2; flip angle, 12°; acquisition time, 11 s for each dataset) of the liver were acquired nonenhanced as well as contrast enhanced in the arterial phase (25-s delay), portal venous phase (33-s delay), and venous phase (41-s delay) without respiratory gating.

Image Evaluation and Data Analysis

Ultrasound, MR, and CT images were each assessed by different radiologists, whereas PET and PET/CT images were read by a nuclear medicine physician in conjunction with a radiologist. Image assessment was performed qualitatively for areas of altered contrast enhancement on morphologic imaging procedures and for regions of altered glucose utilization on functional imaging. Qualitative image assessment was performed by comparing the periphery of the ablative necrosis with the untreated liver parenchyma and rated on a 3-point scale: 1 = homogeneous contrast enhancement/glucose metabolism of region surrounding the necrosis (lesion periphery) compared with normal (untreated) liver paren-

chyma; 2 = mild increase in contrast enhancement/glucose utilization surrounding the ablative necrosis compared with normal liver parenchyma; 3 = strong increase in contrast enhancement/glucose utilization of tissue surrounding the necrosis compared with normal liver parenchyma.

In addition, all images were assessed quantitatively. The lesion size was assessed based on measurements of both small-axis and large-axis diameters. To determine the effect of RF-ablation on contrast enhancement, 2 ratios were determined for MRI and CT based on measurements of signal intensity by applying regions of interest (ROIs) to the center of the lesion, the lesion periphery, and an area of normal liver parenchyma.

The contrast enhancement ratio between the center of ablative necrosis and the normal liver parenchyma is:

$$r_{c/p} = \frac{\text{contrast enhancement lesion center}}{\text{contrast enhancement normal parenchyma}}.$$

The contrast enhancement ratio between the periphery of ablative necrosis and the normal liver parenchyma is:

$$r_{p/p} = \frac{\text{contrast enhancement lesion periphery}}{\text{contrast enhancement normal parenchyma}}.$$

Contrast enhancement was quantified in Hounsfield units for CT and signal intensity for MRI. Software for quantification of contrast enhancement on US images has not been available commercially yet.

To determine the effect of treatment on PET tracer quantification in the region of the ablative necrosis and in the periphery of the necrosis, 2 ratios were determined in analogy to the other imaging procedures by determination of ROIs.

The tracer activity ratio between the center of ablative necrosis and the normal liver parenchyma is:

$$r_{c/p} = \frac{\text{activity concentration lesion center}}{\text{activity concentration normal parenchyma}}.$$

The tracer activity ratio between the periphery of ablative necrosis and the normal liver parenchyma is:

$$r_{p/p} = \frac{\text{activity concentration lesion periphery}}{\text{activity concentration normal parenchyma}}.$$

Histopathology

After RF-ablation and subsequent imaging, 3 animals were sacrificed for histopathologic evaluation of the ablative necroses. Liver tissue samples from the ablated regions and the untreated liver parenchyma were fixed in 4% buffered formalin and embedded in paraffin. Three-micrometer sections were stained with hematoxylin–eosin, periodic acid–Schiff, and Elastica–van Gieson. The lesions were photodocumented using a microscope (Eclips 80i; Nikon) equipped with a digital camera (DXM 1200F; Nikon). Slides were evaluated by a pathologist for areas of necrosis, regeneration, scar formation, and an inflammatory reaction.

RESULTS

RF-Ablation

Blood glucose levels were found to be normal before the intervention and all imaging procedures. RF-ablation was performed without complications in all 10 pigs. In 1 pig, only 1 RF-ablation could be performed due to a hypoplastic left hepatic lobe. Therefore, data analysis was based on 19 lesions in 10 pigs.

Mean Lesion Size

According to the measurement of tissue samples, the mean lesion size was found to measure 3.9 cm in the large-axis diameter and 2.7 cm in the small-axis diameter. PET slightly underestimated lesion size, whereas US, CT, MRI, and PET/CT determined both diameters equally well. Underestimation of the lesion size on PET alone was based on blurring of the lesions' margins (Fig. 1). The mean large-axis and small-axis diameters of RF-induced lesions as determined with the different imaging procedures are summarized in Table 1.

Qualitative Image Analysis

On CT, MRI, and US, the center of the ablative necrosis was characterized as a hypodense/hypointense/hypoechoic area compared with normal liver parenchyma. After the administration of contrast agent, enhancement was identified in the arterial phase surrounding all ablative necroses on US, CT, and MR images (Fig. 1). The mean qualitative score of this rim-like contrast enhancement amounted to 2.4 ± 0.5 for MRI, 2.7 ± 0.5 for CT, and 2.3 ± 0.5 for US based on the 3-point scale. When assessing PET images qualitatively, the area of necrosis was characterized by decreased glucose metabolism. Homogeneous tracer utilization was found in all livers of ablated pigs when comparing liver tissue surrounding the necrosis with the normal liver parenchyma (Fig. 1). There were no areas of a focal or rim-like increases in glucose metabolism adjacent to the ablative necrosis. Qualitative evaluation revealed a mean score of 1 ± 0 for qualitative analysis (Fig. 2).

Quantitative Image Analysis

The necrotic zone was characterized by less echogenicity/density/signal compared with contrast-enhanced liver parenchyma on all morphologic imaging datasets. The mean $r_{c/p}$ was 0.77 ± 0.10 for CT and 0.59 ± 0.19 for MRI. On PET, the necrotic center was depicted as a cold spot surrounded by homogeneous glucose metabolism of nontreated liver tissue leading to ratios of $r_{c/p} = 0.65 \pm 0.11$.

Liver tissue surrounding the necrosis revealed increased contrast enhancement on CT and MRI when assessed quantitatively. Ratios amounted to $r_{p/p} = 1.57 \pm 0.20$ for CT and $r_{p/p} = 1.57 \pm 0.19$ for MRI. The mean diameter of this rim measured 4.8 ± 1.6 mm on CT, 3.1 ± 0.7 mm on MRI, and 3.2 ± 1.3 mm on US images. Quantitative evaluation of the lesion periphery on PET demonstrated homogeneous glucose utilization as compared with normal liver tissue. The ratio $r_{p/p}$ was found to be 1.05 ± 0.08 for PET (Fig. 3).

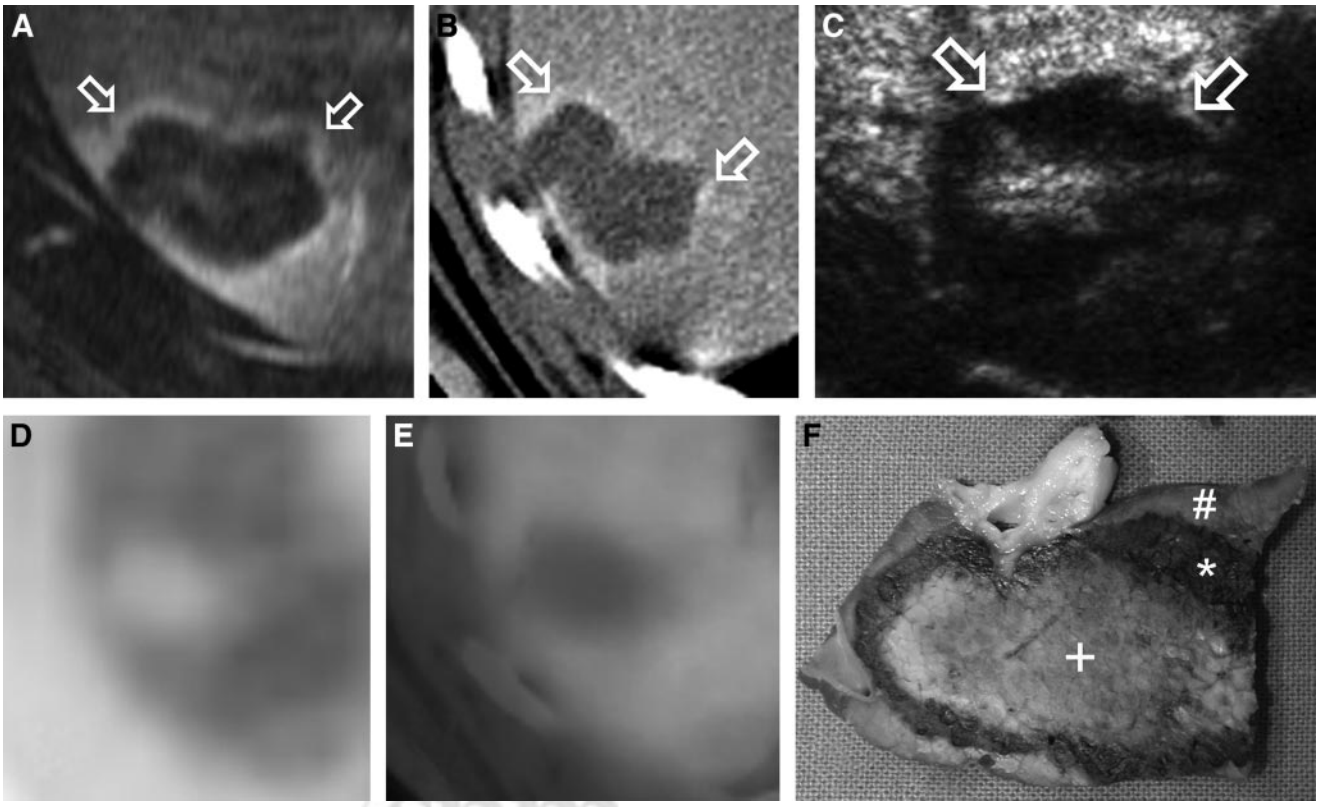

FIGURE 1. Transversal images immediately after RF-ablation. Rim-like increase of contrast enhancement in arterial phase (arrows) was detected on MRI (A), CT (B), and US (C). Functional data provided by PET (D) and PET/CT (E) demonstrated an area of decreased ^{18}F-FDG uptake surrounded by homogeneous tracer distribution. Macroscopic tissue sample generated after sacrificing 1 animal (F) shows central necrosis (+), adjacent rim of blood-filled sinusoids (*), and macroscopically normal liver parenchyma (#). Note blurred margins of lesion on PET (D) leading to slight underestimation of lesion size.

TABLE 1
Mean Maximal Diameters (Large-Axis Measurement) and Mean Minimal Diameters (Small-Axis Measurement) of RF-Induced Necrotic Zone as Determined by Different Imaging Procedures

Imaging procedure	Measurement 1		Measurement 2	
	Maximal diameter (cm)	Minimal diameter (cm)	Maximal diameter (cm)	Minimal diameter (cm)
US	3.7 ± 0.7	2.5 ± 0.6	3.6 ± 0.6	2.4 ± 0.4
CT	3.8 ± 0.7	2.5 ± 0.5	3.8 ± 0.7	2.5 ± 0.5
MRI	3.8 ± 0.9	2.5 ± 0.6	4.1 ± 0.9	2.7 ± 0.7
PET	3.4 ± 0.8	2.3 ± 0.5	—	—
PET/CT	3.8 ± 0.7	2.5 ± 0.3	—	—

For US, CT, and MRI, measurement 1 represents determination of lesion size in venous phase, and measurement 2 represents lesion size in arterial phase. For PET and PET/CT, only 1 measurement was performed (measurement 1). Measurements are expressed as mean ± SD.

Histopathology

Three different zones were detected when evaluating the ablative site histopathologically. A central zone demonstrated early signs of tissue necrosis. A transitional zone showed sinusoids engorged with blood caused by outflow

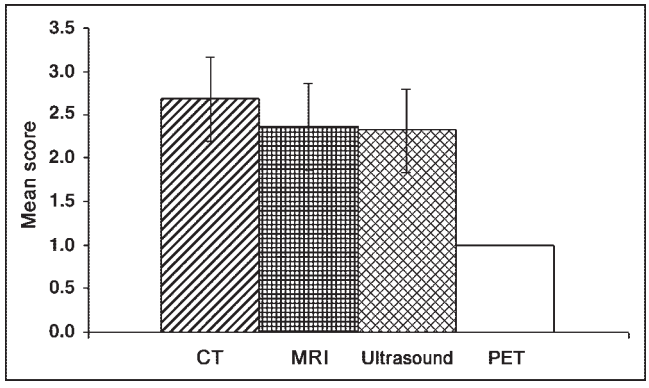

FIGURE 2. Qualitative image analysis according to 3-point scale revealed increased contrast enhancement in periphery of induced necrosis when compared with normal liver parenchyma with all morphologic imaging procedures. On PET, no increase in glucose metabolism was found, leading to a score of 1 in all 19 lesions.

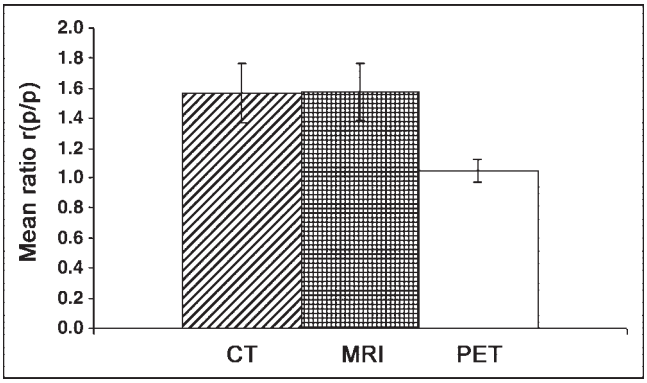

FIGURE 3. Quantitative image analysis by determination of ratio of contrast enhancement of lesion periphery/contrast enhancement of normal liver parenchyma for CT and MRI as well as ratio of activity concentration of lesion periphery/activity concentration of normal liver parenchyma on PET. Due to rim-like increase of contrast enhancement in periphery of necrosis, ratios are elevated for morphologic imaging procedures, whereas homogeneous tracer distribution on PET led to a mean ratio of 1.05 for functional data analysis.

obstruction due to the central ablative necrosis. A peripheral zone demonstrated mild reactive changes (Fig. 4).

DISCUSSION

RF-ablation has an effect on normal liver tissue in the periphery of the induced necrosis. Immediately after the intervention, local hyperemia caused by outflow obstruction leads to increased contrast enhancement on all morphologic imaging procedures, rendering detection of residual tumor difficult. On functional imaging, however, homogeneous tracer distribution surrounding the area of focally decreased glucose utilization can be detected. Based on homogeneous tracer distribution, residual tumor demonstrating as a hot spot should be easily detected with PET and PET/CT.

Imaging follow-up of patients undergoing interventional liver therapy is generally based on contrast-enhanced CT, MRI, or US (*4,25*). While hyperemia is responsible for increased contrast enhancement immediately after the RF ablation, tissue regeneration in the periphery of the necrotic zone results in a persistence of increased contrast uptake for a longer period of time (*14,15*). Both phenomena prohibit the identification of residual tumor with these techniques in the time after RF ablation. Some authors, therefore, recommend waiting 6–12 wk before performing follow-up procedures to avoid physiologic contrast enhancement (*4,14*). To minimize the risk of tumor spread, the diagnosis of residual tumor after RF-ablation should be made as soon as possible, however.

All morphologic imaging procedures demonstrated areas of increased contrast enhancement in the arterial phase surrounding the region of RF-ablation. Hepatocellular carcinoma as well as metastases from neuroendocrine tumors also typically present as lesions with early arterial contrast enhancement (*26*). When performing RF ablation in patients with these malignancies, differentiation of early arterial hyperemia from residual tumor will be difficult. Hence, a close follow-up of the ablative site with CT, MRI, or US over at least 1 y is required for detection of local tumor recurrence (*9,27*).

When assessing patients with liver metastases from tumors of the gastrointestinal tract, peripheral hyperemia is not expected to cause interpretative problems. Hepatic metastases from gastrointestinal tumors are mostly imaged as hypodense (CT), hypointense (MRI), or hypoechoic (US) lesions surrounded by normal contrast-enhanced liver parenchyma. In these cases, the rim-like contrast enhancement will not be mistaken for residual tumor—thus, not compromising image assessment.

In patients with ^{18}F-FDG-positive lesions, ^{18}F-FDG PET, and ^{18}F-FDG PET/CT can be used for therapy follow-up of patients undergoing interventional liver therapy. In 2 initial series, ^{18}F-FDG PET was found to be more sensitive regarding the detection of residual tumor and tumor recurrence than morphologic imaging procedures (*16,17*). The positive predictive value for residual tumor after RF-ablation was reported to be 100% (*16*). Though these results are intriguing, neither study reports the time interval between liver intervention and PET. This time interval is, however, important, as regenerative tissue alteration in the periphery of the ablative necrosis has been shown to present as areas of focally increased glucose metabolism (*20*). Tissue regeneration can be found as early as 3 d after RF-ablation (*2*). Therefore, PET assessment of the effect of RF-ablation should be performed early.

Immediately after RF-ablation, no tissue regeneration was detected on histopathologic examination. As theorized, all ablative sites were characterized by decreased glucose metabolism surrounded by homogeneous liver parenchyma on PET and PET/CT. Other effects on ^{18}F-FDG uptake in the periphery of the necrosis must be considered. Partial-volume effects, for example, may cause apparently de-

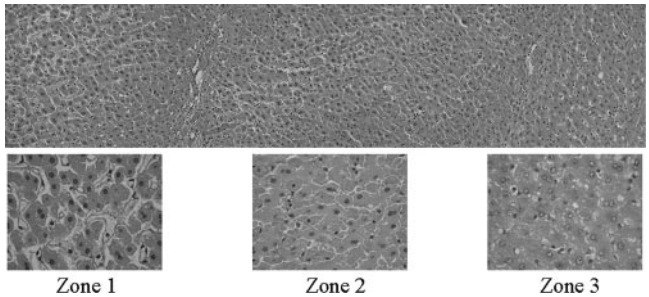

FIGURE 4. Fragmentation of liver plates were visible in center of lesion (zone 1), demonstrating early signs of necrosis. No blood cells were detected in zone 1 due to occlusion of sinusoids caused by edema of hepatocytes. This edema, furthermore, led to widening of space of Disse. In transitional zone (zone 2), sinusoids were engorged with blood caused by outflow obstruction. Peripheral zone (zone 3) is characterized by unspecific vacuolar transformation of cytoplasm of hepatocytes as sign of reactive changes.

creased tracer uptake in the periphery of the necrosis, whereas local hyperperfusion could be expected to increase glucose uptake based on an increase in tracer supply. Furthermore, local hyperthermia may affect the glucose metabolism of liver cells adjacent to the ablative site. All of these potential influences on the local ^{18}F-FDG distribution did, however, not result in a decrease or increase in glucose uptake. Thus, the overall ("Netto") influence of all of these effects seems to amount to zero. Based on the homogeneous glucose utilization of normal liver parenchyma, residual tumor should become detectable as a hot spot or rim-like increase in glucose metabolism in the periphery of the ablative site. The additional CT component of combined PET/CT will ensure the accurate localization of the residual tumor site. This additional information must be considered crucial for the success of reinterventions to eliminate the residual tumor. By localizing the viable tumor tissue with respect to adjacent blood vessels, the gallbladder, and other structures, PET/CT data do not merely guide the ablative device to the most optimal position but also minimize the risk of complications (*20*). Hence, it seems likely that PET/CT will be of substantial benefit for an early assessment of therapy response to RF-ablation. Clearly, however, further studies addressing this issue in a clinical setting will be required. When assessing PET/CT in clinical routine, the cost effectiveness of the combined imaging approach when compared with morphologic imaging procedures will be an important issue. Apart from the cost of the imaging procedures, a thorough cost analysis will have to include items such as potential reinterventions, further follow-up procedures, additional therapy required, and patient survival.

CONCLUSION

This study documents that the detection of residual tumor with PET and PET/CT immediately after RF-ablation of liver lesions will not be hampered by increased cell metabolism. In contrast to CT, MRI, and US, the rim surrounding the ablative necrosis remained unaffected after the administration of ^{18}F-FDG. As this initial study merely examined healthy animals, further research will have to evaluate whether this potential advantage of PET and PET/CT over morphologic imaging procedures translates into a more accurate assessment of residual tumor after RF-ablation.

ACKNOWLEDGMENTS

The authors thank Sandra Massing, RT, and Silke Bosk, RT, for conducting the MRI examinations. We gratefully acknowledge the substantial support of Mr. Dirk Lahmer, MSc, in providing the ^{18}F-FDG for the animal experiments.

REFERENCES

1. Dupuy DE, Goldberg SN. Image-guided radiofrequency tumor ablation: challenges and opportunities—part II. *J Vasc Interv Radiol.* 2001;12:1135–1148.
2. Goldberg SN, Dupuy DE. Image-guided radiofrequency tumor ablation: challenges and opportunities—part I. *J Vasc Interv Radiol.* 2001;12:1021–1032.
3. Gazelle GS, Goldberg SN, Solbiati L, Livraghi T. Tumor ablation with radiofrequency energy. *Radiology.* 2000;217:633–646.
4. Lencioni R, Cioni D, Bartolozzi C. Percutaneous radiofrequency thermal ablation of liver malignancies: techniques, indications, imaging findings, and clinical results. *Abdom Imaging.* 2001;26:345–360.
5. Adamus R, Tesdal IK, Georgi M. Percutaneous alcohol instillation therapy (PAI) and chemoembolization in extensive hepatocellular carcinoma [in German]. *Rofo Fortschr Geb Rontgenstr Neuen Bildgeb Verfahr.* 1997;166:173–175.
6. Bartolozzi C, Lencioni R, Ricci P, Paolicchi A, Rossi P, Passariello R. Hepatocellular carcinoma treatment with percutaneous ethanol injection: evaluation with contrast-enhanced color Doppler US. *Radiology.* 1998;209:387–393.
7. Solbiati L, Ierace T, Tonolini M, Osti V, Cova L. Radiofrequency thermal ablation of hepatic metastases. *Eur J Ultrasound.* 2001;13:149–158.
8. Livraghi T, Goldberg SN, Solbiati L, Meloni F, Ierace T, Gazelle GS. Percutaneous radio-frequency ablation of liver metastases from breast cancer: initial experience in 24 patients. *Radiology.* 2001;220:145–149.
9. Solbiati L, Livraghi T, Goldberg SN, et al. Percutaneous radio-frequency ablation of hepatic metastases from colorectal cancer: long-term results in 117 patients. *Radiology.* 2001;221:159–166.
10. Antoch G, Kuehl H, Vogt FM, Debatin JF, Stattaus J. Value of CT volume imaging for optimal placement of radiofrequency ablation probes in liver lesions. *J Vasc Interv Radiol.* 2002;13:1155–1161.
11. Solbiati L, Ierace T, Goldberg SN, et al. Percutaneous US-guided radio-frequency tissue ablation of liver metastases: treatment and follow-up in 16 patients. *Radiology.* 1997;202:195–203.
12. Rhim H, Goldberg SN, Dodd GD 3rd, et al. Essential techniques for successful radio-frequency thermal ablation of malignant hepatic tumors. *Radiographics.* 2001;21:17–39.
13. Goldberg SN, Gazelle GS, Compton CC, Mueller PR, Tanabe KK. Treatment of intrahepatic malignancy with radiofrequency ablation: radiologic-pathologic correlation. *Cancer.* 2000;88:2452–2463.
14. Goldberg SN, Gazelle GS, Mueller PR. Thermal ablation therapy for focal malignancy: a unified approach to underlying principles, techniques, and diagnostic imaging guidance. *AJR.* 2000;174:323–331.
15. Goldberg SN, Mallery S, Gazelle GS, Brugge WR. EUS-guided radiofrequency ablation in the pancreas: results in a porcine model. *Gastrointest Endosc.* 1999; 50:392–401.
16. Anderson GS, Brinkmann F, Soulen MC, Alavi A, Zhuang H. FDG positron emission tomography in the surveillance of hepatic tumors treated with radiofrequency ablation. *Clin Nucl Med.* 2003;28:192–197.
17. Langenhoff BS, Oyen WJ, Jager GJ, et al. Efficacy of fluorine-18-deoxyglucose positron emission tomography in detecting tumor recurrence after local ablative therapy for liver metastases: a prospective study. *J Clin Oncol.* 2002;20:4453–4458.
18. Shreve PD, Anzai Y, Wahl RL. Pitfalls in oncologic diagnosis with FDG PET imaging: physiologic and benign variants. *Radiographics.* 1999;19:61–77.
19. Cook GJ, Maisey MN, Fogelman I. Normal variants, artefacts and interpretative pitfalls in PET imaging with 18-fluoro-2-deoxyglucose and carbon-11 methionine. *Eur J Nucl Med.* 1999;26:1363–1378.
20. Antoch G, Freudenberg LS, Beyer T, Bockisch A, Debatin JF. To enhance or not to enhance? ^{18}F-FDG and CT contrast agents in dual-modality ^{18}F-FDG PET/CT. *J Nucl Med.* 2004;45(suppl):56S–65S.
21. Schmidt KH, Muller U, Horer W, Braatz R. Changes in the pattern of microsomal fatty acids in rat liver after thermal injury and therapeutic intervention. *Burns Incl Therm Inj.* 1988;14:25–30.
22. Magic Z, Ristovic B, Pantelic D. Effect of non-lethal scalding on the amount of DNA and RNA in rat liver. *Burns Incl Therm Inj.* 1986;12:172–175.
23. Lencioni R, Goletti O, Armillotta N, et al. Radio-frequency thermal ablation of liver metastases with a cooled-tip electrode needle: results of a pilot clinical trial. *Eur Radiol.* 1998;8:1205–1211.
24. Kinahan PE, Townsend DW, Beyer T, Sashin D. Attenuation correction for a combined 3D PET/CT scanner. *Med Phys.* 1998;25:2046–2053.
25. Tacke J. Percutaneous radiofrequency ablation: clinical indications and results [in German]. *Rofo Fortschr Geb Rontgenstr Neuen Bildgeb Verfahr.* 2003;175:156–168.
26. Paul SB, Gulati MS. Spectrum of hepatocellular carcinoma on triple phase helical CT: a pictorial essay. *Clin Imaging.* 2002;26:270–279.
27. Solbiati L, Livraghi T, Ierace T, Meloni F, Goldberg SN. Local control of focal liver malignancies treated with RF ablation: initial report of the Italian Multicenter Cooled-Tip RF Study Group [abstract]. *Radiology.* 2000;217:27.